INVESTIGATION OF SIZE AND SPATIAL DISTRIBUTION OF DEFECTS IN S2 GLASS FIBERS USING CONTINUOUS FIBER BENDING TEST METHOD

Ahmad Abu-Obaid[1], Raja Ganesh[1,2] and John W. Gillespie, Jr. [1,2,3,4]

[1]Center for Composite Materials, University of Delaware, DE, USA

[2]Department of Mechanical Engineering, University of Delaware, DE, USA

[3]Department of Materials Science and Engineering, University of Delaware, DE, USA

[4]Department of Civil and Environmental Engineering, University of Delaware, DE, USA

Corresponding author: Ahmad Abuobaid, abuobaid@udel.edu

ABSTRACT

A novel continuous fiber bending test method was developed to measure the size and spatial distribution of defects in glass fiber. For this test method, a lubricated single S2-glass fiber is placed between two Kapton carrier films and subjected to pure bending deformation over a loading surface of prescribed radius of curvature that generates flexural strain in the fiber and creates fiber fracture at the largest surface defect locations. Tests are conducted over 870 mm of fiber length to generate statistical data. The same sample is then tested with a smaller radius of curvature surface to generate a higher flexural strain level to trigger additional fiber fractures at surface defects of smaller size. This sequence is repeated for loading surfaces with radii of curvatures ranging from ranges from 350 μm to 25 μm. For the 10-micron S2-glass fiber this corresponds to flexural strains range of 1.4 % to 11.6 %. By measuring the location of fiber breaks at each radius of curvature, the number of surface defects and the associated spacings between the defects are obtained for each level of flexural strain. The associated defect size is calculated using fracture mechanics. The test method generates a map of the defect size and spacing along the fiber length for the first time.

Keywords: S2 glass fiber, defects, flexural testing

1. INTRODUCTION

It is well known that surface defects can arise during fiber spinning, application of fiber sizing and weaving operations [1-3]. The effects of defects have been experimentally measured through single fiber tension testing and exhibit a strength distribution that is dependent on the gage length. This behavior has traditionally been explained by Weibull strength theory [4] that assume a size distribution of defects exist within the fiber length and failure occurs at the largest defect (i.e. weakest link). In this case as the gauge length of a fiber decreases, the mean of the strength distribution shifts to higher strength values while the distribution broadens to include low strength associated with the large defects. The theory has some limitations in that the location of the defects are not known and the minimum gauge length in which the theory is applicable is not known (the minimum length is defined as the length that contains the entire defect size population). The test method developed in this study provides a methodology to determine both the defect size distribution and spatial location of those defects. This study was motivated by problems requiring this level of detail such as breakage of short fiber subjected to flexural deformation during

processing [5] that can reduce fiber aspect ratio and mechanical properties as well as the tensile loading of unidirectional (UD) composites where fiber breaks lead to localization and tensile failure of the composite.

To generate data on defect size and location required for multi-scale modeling, a unique test method was developed where a long fiber is continuously subjected to pure bending strain allowing for defect size and location to be measured. The novelty of this method allows one to map the physical defects onto the fiber surface.

2. MATERIALS

In this work, AGY S2 glass fibers (463-AAA-1250) were evaluated. These fibers have a nominal tensile strength of 3.7-4.3 GPa [6] for a standard gage length of 10 mm. The fiber diameter was measured in this effort as 9.90±0.45 µm. For bending tests, stainless steel wires (AISI 316L) with different diameters, supplied by Goodfellow Corporation are used as the loading surface with controlled radius of curvature. The diameters of the wires used in this study are 700 µm, 500 µm, 200 µm, 150 µm, 100 µm and 50 µm.

3. EXPERIMENTAL METHODS

3.1 Bending test setup

In this effort, bending tests were conducted on the samples using a specially developed setup (see Figure 1). The major components of this setup are a razor blade (supplied by IRWIN Company) with mounted stainless steel wire, rollers, a syringe pump to pull the sample at constant speed, a hanging weight (60 g) to ensure uniform contact between the sample and wire, 44.5 N load-cell to monitor the load while the sample is being pulled over the wire and confocal microscope to measure the actual curvature of the sample around the wire during bending test. Moreover, the blade/wire assembly was vertically placed in a fixture (blade holder), where the height of the wire relative to the center of the line of the rollers can be adjusted to ensure the contact length of the sample undergoing bending over the wire is controlled (see Figure 1).

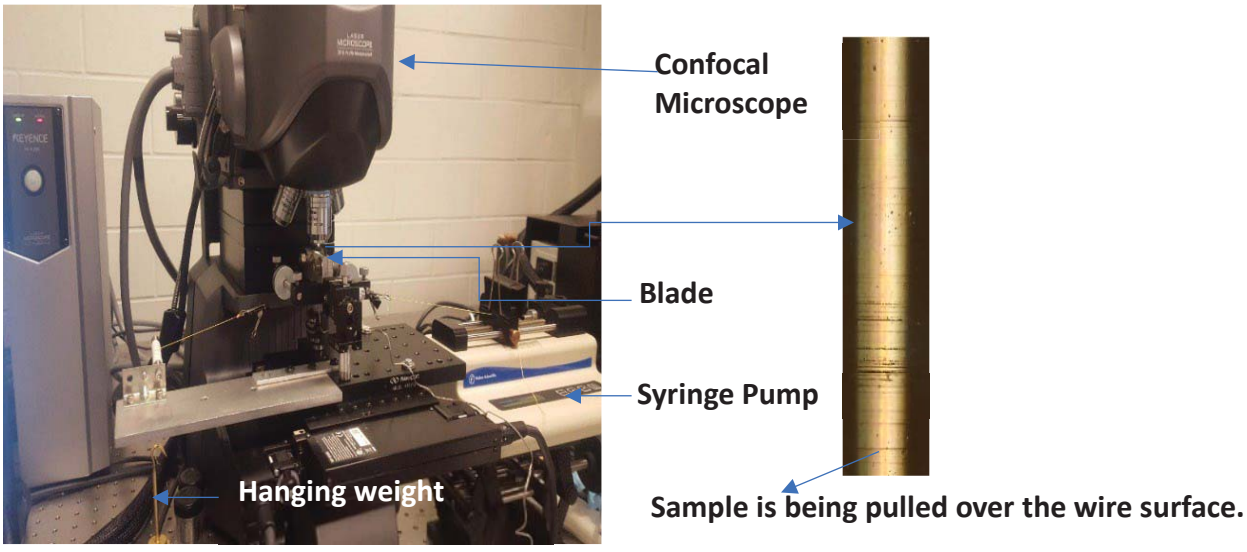

Figure 1: Continuous fiber bending test setup

One of the key components in bending test setup is the blade-wire assembly. In this the effort, the stainless-steel wire was mounted on the tip of the razor blade using an alignment fixture shown in Figure 2. The major components of this fixture are a 3D stages and two height adjustable metal rods allowing one to achieve a better positioning control of wire mounting on the blade tip. Prior to the mounting procedure, the tip of the stainless-steel blade was polished to a width which is comparable to wire diameter being used. Wire mounting procedure was carried out as follows (see Figure 2). The blade was mounted horizontally to the surface of a metal support using a double side tape and then the assembly was placed horizontally on the surface of the 3D-stage. A 40 cm long wire was cut and aligned along the polished blade tip, where the wire was straightened by attaching its ends with hanging weights. Using the 3D stage and a magnifier, the blade tip was carefully moved upward toward the aligned wire till both the tip and the wire were in contact (see a close-up Fig.2). Finely, the tip was adhered to the aligned wire using the Loctite 430 adhesive. It is noteworthy that the ends of the mounted metal wire were secured using a masking tape. Using the same procedure, blades with different wire diameters (700 µm-50 µm) were prepared.

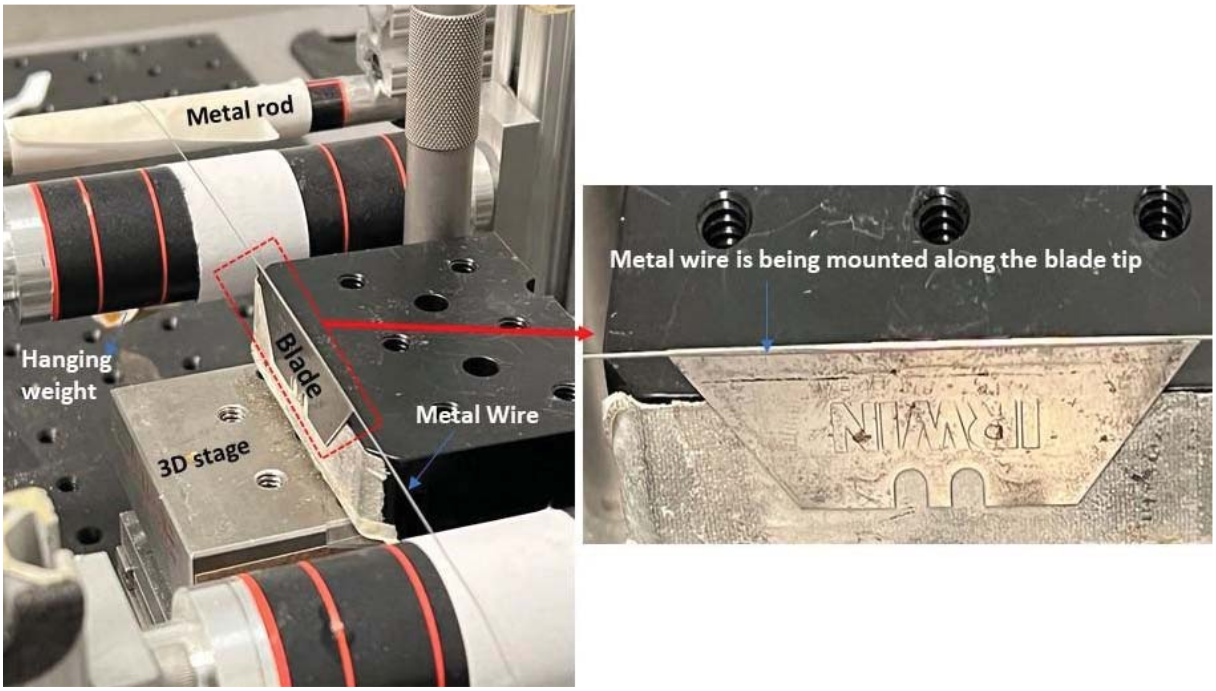

Figure 2: Alignment fixture used in the steel wire mounting procedure on the blade tip.

3.2 Test sample preparation and bending test procedure

For continuous fiber bending test, a 20 cm long single glass monofilament was carefully extracted from the tow and sandwiched between Kapton film (25 cm long and ~13 µm thick) and Kapton tape with thickness of ~29 µm (Figure 3). The sample preparation was carried out according to following procedure. Kapton film with thickness of 13 µm was placed on a flat plate and then the

fiber was aligned along the film center line. Finally, the Kapton tape with thickness of 29 µm was carefully placed and aligned along the assembly resulting in a cross-section of the sample shown in Figure 3. In this sample preparation, the Kapton film with thickness larger than the fiber diameter functions as frictionless medium between the fiber and the Kapton film during fiber bending. At least 39 samples were prepared.

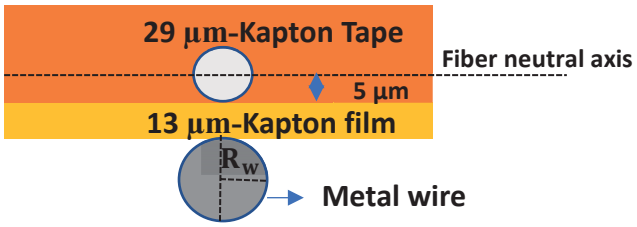

Figure 3: Schematic for the cross-section of the prepared bending test sample

The sample (film/fiber/tape) was mounted in the setup as shown in Figure 1 by gripping one sample end with the hanging weight (70 g) and the other end with the syringe pump, where the film side of sample always was facing the wire surface. Then, the sample was pulled over the wire surface by a constant speed of 0.33 mm/min covering 20 mm distance along the sample. The motion of the sample during bending test was monitored using the confocal microscope to ensure a smooth motion while the sample pulled over the wire surface. Representative image for a sample during bending tests is shown in Figure 4, where the fiber exhibits breaks on the surface.

In this effort, bending tests were performed at different radii of curvatures ranging from 350 µm to 25 µm on the same sample in sequential manner. After each subsequent radius the fiber breaks were imaged using high-resolution microscope (see Figure 4) and defect locations were measured with respect to a reference point.

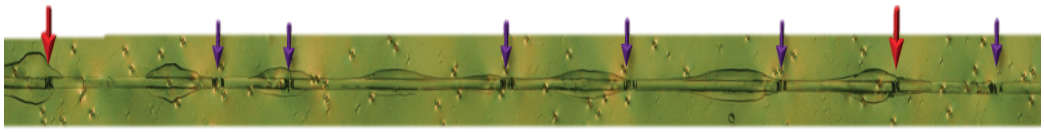

Figure 4: Representative image for the breaks appeared on the fiber surface during bending test.

4. DATA REDUCTION

4.1 Effective radius of curvature, maximum bending stress and strain

The schematic cross-section of bending test sample is shown in Figure 3, where the fiber with radius of 5 µm is being imbedded in the adhesive of Kapton tape and subjected to the bending stress via the Kapton film when the sample is moving over the wire surface with radius of R_w (see Figure 3). So, bending of the sample over the wire surface results in a curvature of the fiber via the Kapton film. Hence, the effective radius of curvature R_{eff} can be given as

$$R_{eff} = R_w + R \quad (1)$$

Where R =film thickness + fiber radius =18 μm.

Applying Equation 1, the maximum bending strain (ε_{bm}) for the fiber with radius (r =5 μm) measured from the neutral axis can be calculated as

$$\varepsilon_{bm} = \frac{r}{R_{eff}} \quad (2)$$

and the maximum bending stress σ_{bm} can be calculated as

$$\sigma_{bm} = E_f \varepsilon_{bm} \quad (3)$$

Where E_f =90 GPa, which is the elastic modulus for S2 glass fiber.
Table 1 lists the values of maximum bending stress and their intervals for each effective radius of curvature (R_{eff}).

4.2 Defect size

In this effort, we assumed that the breaks measured along the fiber are due to the existence of surface cracks having a penny-shape geometry. From fracture mechanics biases [7], the size of surface crack (a) in a solid cylinder during uniform flexural loading (bending) can be given as

$$a = \frac{1}{\pi}\left(\frac{K_c}{F_1 \sigma}\right)^2 \quad (4)$$

Where Kc is the critical stress intensity factor, σ is the bending stress and F_1 is the specimen geometric parameter. For S2 glass fibers, Kc= 1.64 MPa $m^{1/2}$ [8] and F_1=0.6.

4.3 Spacing between the defects

The location of breaks in each 2 cm long sample tested at a given effective radius of curvature (R_{eff}), were measured with respect to a reference point on the fiber. Then, the cumulative distances of the defects appeared within the total length of 780 mm (all 39 samples) were constructed. So, the cumulative distance (D_{ij}) for j^{th} break appeared in the i^{th} sample was defined in micrometers unit as

$$D_{ij} = 2000 * (i - 1) + D_{ij}^* \quad (5)$$

Where i is the sample number (i=1, ….39), j is an integer number, and D_{ij}^* is the individual break location in the i^{th} sample. The plot of maximum bending stress or defect size versus cumulative distance represent the mathematical map of the defects along the fiber.

For all samples tested at same radius of curvatures, the spatial differences between the defects (ΔL) (i.e fragment lengths) were defined as the differences between each two successive break locations.

Furthermore, the statistical distributions of spacings between the defects were generated for each maximum bending stress.

Table 1: Number of defects, defect size, maximum bending strain, maximum bending stress (upper limit of the stress interval) and bending stress intervals obtained at different effective radii of curvatures (R_{eff}) for S2 glass fiber.

D (μm)	R_{eff} (μm)	σ_{bm}(GPa) interval	σ_{bm}(GPa)	ε_{bm}(%)	Defect size (nm)	No. of Defects* Nc	No. of Defects* N_I
700	368	0-1.2	1.22	1.36	1572	5	5
500	268	1.2-1.7	1.68	1.87	829	7	2
300	168	1.7-2.7	2.68	2.98	326	22	15
200	118	2.7-3.8	3.81	4.24	161	40	18
150	93	3.8-4.8	4.84	5.38	100	92	52
100	68	4.8-6.6	6.62	7.35	53	189	97
50	43	6.6-10.5	10.47	11.63	21	286	97

*N_C is defined as the cumulative number of defects measured at a given stress level and below that level. N_I is defined as difference between two successive Nc values.

5. RESULTS AND DISCUSION

5.1 Size and number of defects

For each sample tested at each radius of curvature, the breaks that occur along the fiber over 780 mm length (20 mm x 39 samples) were imaged and counted. These breaks correspond to a specific location along the fiber and each break is associated with a specific flexural strength/flexural strain to failure and a unique defect size using fracture mechanics as explained above. Using Equation 4, defect size was calculated and listed in Table 1 for each maximum bending stress interval. The defect size ranges from 21-1572 nm in the bending stress range of 1.22- 10.46 GPa and strain range of 1.36%-11.63%.

The number of breaks represents the number of defects that exist on tension surface of the fiber. In total, 39 samples (2 cm long) were subjected to flexural loading at seven different radii of curvature. The total number of defects after each loading are measured and given in Table 1. The total (cumulative) number of defects (N_C) measured on the confocal microscope totaled 286 fiber breaks after all seven flexural loadings were completed. This corresponds to 37×10^{-5} defects/μm of fiber length.

Based on the methodology of sequential testing of the samples starting at high and progressing to low radius of curvature, the number of defects for each reduction in radius can also be quantified. The difference between two successive N_C values is the number of defects (N_I) that appears in samples tested within the interval of bending stress interval (see Table 1).

Figures 5-6 shows the individual number of defects (N_I) and their normalized values per unit lengths (number of defects/780000 μm) for each bending stress and defects size bin. From these results, the number of defects exhibits a decreasing behavior with decreasing the flexural stress. Recall that lower strength corresponds to the larger defect sizes. Based on our experimental measurements there are only five large (1572 nm) defects in 780 mm of tested fiber. This corresponds to only 5% of the total defects measured (12×10^{-5} /μm). Conversely, the experimental

data shows the number density (number of defects per unit length) of smaller defect sizes increases significantly as the bending strength of the fiber increases, where a 90%-increase in the number density can be obtained at $\sigma_{bm} \geq 4.84$ GPa. While the number density of smaller defect sizes (less than 21 nm) was not measured (25 μm-wire was a practical lower bound on the wire radius), the measured flexural stress approaches the theoretical upper bound on strength given by the MD simulations of Yejoon et al. [9]. This implies that the defect size and number density should reach a maximum level and decreases to zero at the theoretical limit based on bond breakage mechanisms of strength. This behavior is not captured by Weibull statistics which predicts infinite strength when gage length goes to zero.

5.2 Spatial distributions of defects

In addition to the number of fiber breaks, the spatial location of each defect was also measured from the confocal images with respect to a reference point on the fiber (Equation 5). Using this data and associated defect size given in Table 1 for each maximum stress interval, a plot of defect size versus defect location along the 780 mm fiber (mapping of defect) was generated and depicted in Figure 7. This figure shows clearly that as bending stress increases, the defect size gets smaller (based on Equation 4), the number of defects increases and the spacing between defects becomes smaller. These results emphasize that the defect spacing is statistical in nature.

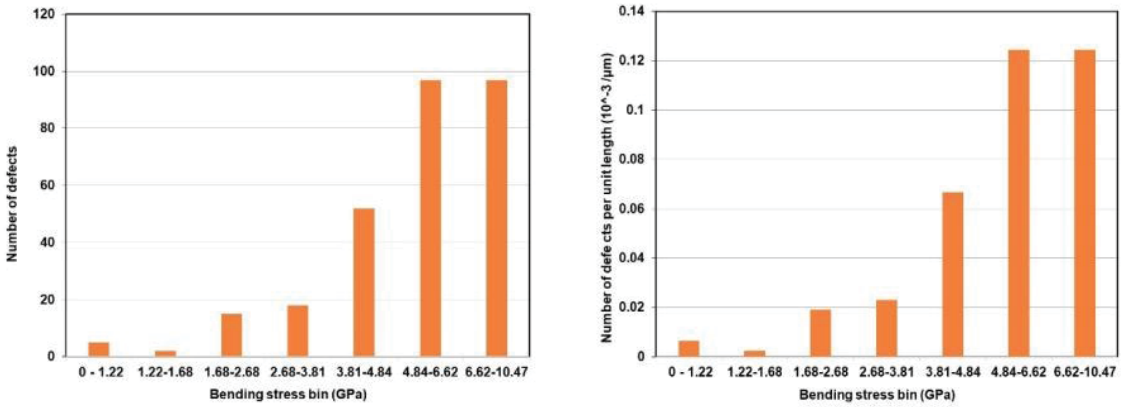

Figure 5: Number of defects (Left) and normalized number of defects per unit length (Right) versus bending stress bin.

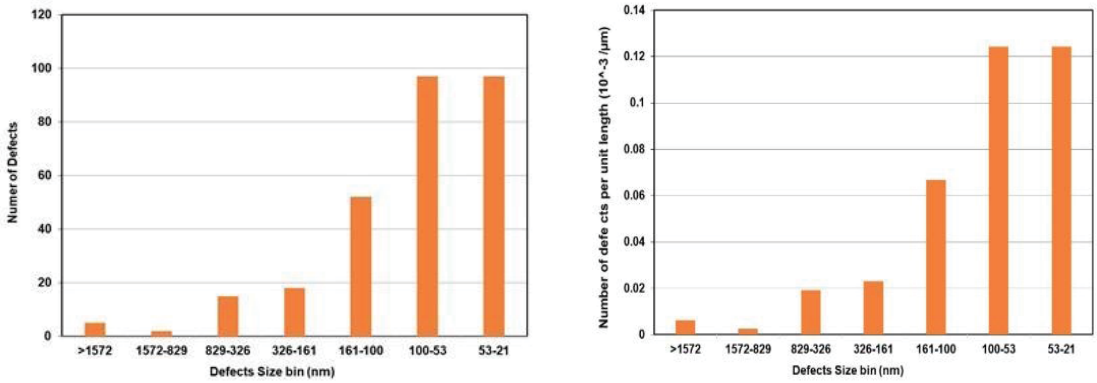

Figure 6: Number of defects (Left) and normalized number of defects per unit length (Right) versus defect size bin.

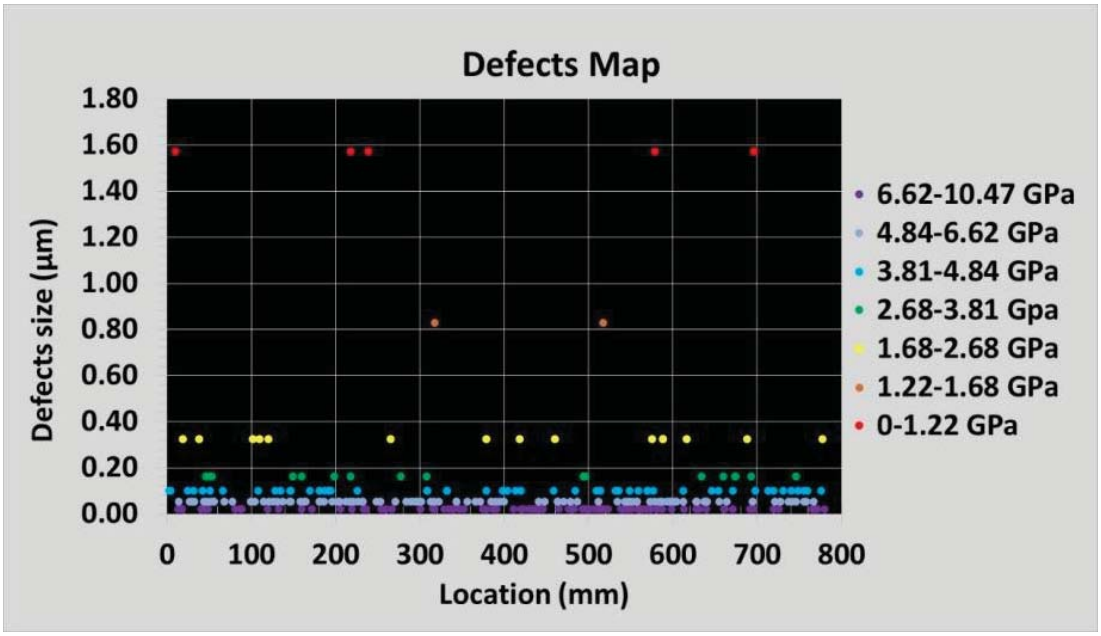

Figure 7: Defect map established for S2 glass fiber over 780 mm.

Based on defect map (Figure 7) results, spatial distributions (histograms) for each defect size were generated using MINITAB software. It was found that experimental data of spatial distributions can be described by lognormal function. Figure 8 shows the lognormal fitting curves of spatial distributions at different maximum bending stress levels and defects size intervals. From this figure, the spacing between the defects at the peak number density of the distributions exhibits shifts from 7654 µm at bending stress of 2.68 GPa to smaller value of 439 µm at higher bending stress of 10.47 GPa. Moreover, the fitting parameters of the lognormal distributions were used to generate a plot of the average spacing versus maximum bending stress (see Figure 9) that can be used to interpolate the spacing between the defects for the same fiber tested at bending stress within the range of 1.22-10.47 GPa.

It is noteworthy that at the lowest flexural stress intervals (1 – 1.68 GPa) there are very few large defects in the 780 mm long fibers (see Figure 7) making it impossible to fit the distribution parameters from the current data set.

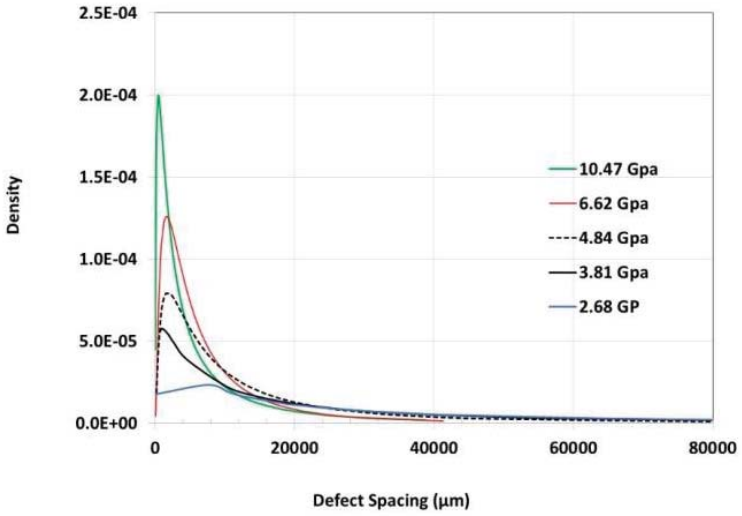

Figure 8: Lognormal fitting curves of spatial distributions generated for S2 glass fibers at different maximum bending stress levels.

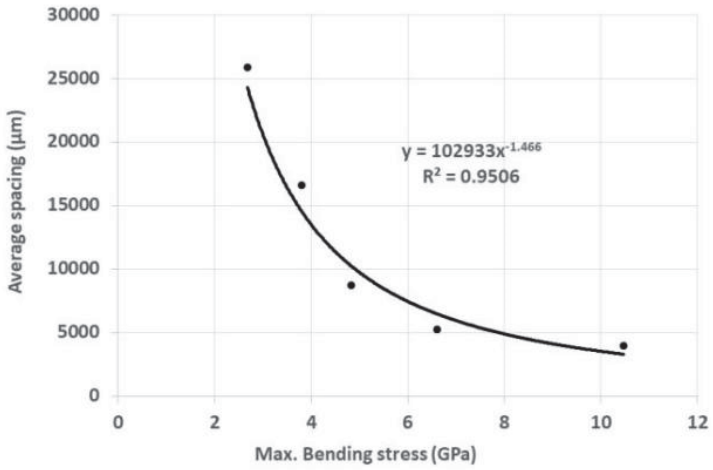

Figure 9: Average spacing between the defects versus maximum bending stress obtained for S2 glass fiber.

6. CONCLUSIONS

A novel continuous bending test method was developed and used to establish the spatial distribution of the defects in S2 glass fibers over length of 780 mm. Defect`s size-location map was established, where higher number of defects with smaller size are activated at higher bending stress levels. The smallest defect size was calculated as 21 nm at the measured flexural stress that approaches the theoretical defect free fiber strength predicted by the MD simulations. Number of defects versus flexural stress and defect size bin data shows that the number density of smaller defect sizes increases significantly as the flexural strength of the fiber increases, where a 90%

increase in the number density was obtained at flexural stress (~10.5 GPa) that approaches the upper bound of MD strength.

Spatial distributions of defects were generated at different stress and defect`s size intervals and their peak values exhibited shifts to lower spacing values with increased bending stress levels. The fitting parameters of these distributions can be used to interpolate the spatial spacing of defects for any given flexural stress within the range of 1.22 Gpa-10.47 GPa.

Overall, the developed test method provides valuable data that can be used for prediction of tensile failure of fibers in unidirectional composites and during processing of short fibers prepregs, where fiber breakage is dependent on size and location of defects in the fibers.

Acknowledgements

This work was sponsored by the Army Research Laboratory accomplished under Cooperative Agreement Number W911NF-12-2-0022. "The views and conclusions contained in this document are those of the authors and should not be interpreted as representing the official policies, either expressed or implied, of the Army Research Laboratory or the U.S. Government. The U.S. Government is authorized to re-produce and distribute reprints for Government purposes notwithstanding any copyright notation herein."

This work is also supported by the National Aeronautics and Space Administration under Grant and Cooperative Agreement No. 80NSSC20M0164, issued through the Aeronautics Research Mission Directorate, Transformative Aeronautics Concepts Program, University Leadership Initiative.

7. REFERENCES

1. Abu-Obaid, S. M. Andersen, J.W. Gillespie Jr, B. Dickenson, A. Watson, G. Chapman, R. A. Coffelt. Effects of weaving on S-2 glass tensile strength distributions. TEXCOMP 9, University of Delaware, Newark, DE, USA. 2008 Oct:13-5.
2. G. Nilakantan, A. Abu Obaid, M. Keefe and J. W. Gillespie Jr. Experimental evaluation and statistical characterization of strength and strain energy distribution of Kevlar yarns: Exploring length -scale and weaving effects. Journal of Composite Materials, vol. 45(17), 2010, pp. 1749-1769. doi: 10.1177/0021998310387667.
3. A. Abu Obaid and J. W. Gillespie Jr. Effects of abrasion on mechanical properties of Kevlar KM2-600 and S glass tows. Textile Research Journal, vol. 89(6), 2019, pp. 989–1002. doi: 10.1177/0040517518760753.
4. W. Weibull. A Statistical Distribution function of wide applicability. ASME Journal of applied mechanics, 1951, pp.18:293–297.
5. P. Simacek, S. G. Advani and J.W. Gillespie Jr. Modeling short fiber deformation in dilute suspension: Fiber deposition process. Composites Science and Technology, vol. 218, 2022. doi: 10.1016/j.compscitech.2021.109149.
6. AGY data sheet: https://www.agy.com/wp-content/uploads/2014/03/463_S-2_Roving-Aerospace_and_Defense.pdf.

7. http://www.afgrow.net/applications/DTDHandbook/Sections/page11_3.aspx#surface_crack_in_a_solid_cylinder.
8. S. C. Chowdhury, E. A. Wise, R. Ganesh, J.W. Gillespie Jr. Effects of surface crack on the mechanical properties of Silica: A molecular dynamics simulation study. Engineering Fracture Mechanics, vol. 207, 2019, pp.207:99-108. doi:10.1016/j.engfracmech.2018.12.025.
9. S. C. Chowdhury and J. W. Gillespie Jr. Mechanical Properties and Damage Analysis of S-glass Fiber: A Reactive Molecular Dynamics Study, submitted to Composites Part B, November 15, 2021.